

****Volume Title****

*ASP Conference Series, Vol. **Volume Number***

****Author****

© ****Copyright Year**** *Astronomical Society of the Pacific*

Parallel-cascade-based mechanisms for heating solar coronal loops: test against observations

Bo Li¹, Haixia Xie¹, Xing Li², and Li-Dong Xia¹

¹*Shandong Provincial Key Laboratory of Optical Astronomy & Solar-Terrestrial Environment, School of Space Science and Physics, Shandong University at Weihai, Weihai 264209, China*

²*Institute of Mathematics & Physics, Aberystwyth University, Aberystwyth SY23 3BZ, UK*

Abstract. The heating of solar coronal loops is at the center of the problem of coronal heating. Given that the origin of the fast solar wind has been tracked down to atmospheric layers with transition region or even chromospheric temperatures, it is worthy attempting to address whether the mechanisms proposed to provide the basal heating of the solar wind apply to coronal loops as well. We extend the loop studies based on a classical parallel-cascade scenario originally proposed in the solar wind context by considering the effects of loop expansion, and perform a parametric study to directly contrast the computed loop densities and electron temperatures with those measured by TRACE and YOHKOH/SXT. This comparison yields that with the wave amplitudes observationally constrained by SUMER measurements, while the computed loops may account for a significant fraction of SXT loops, they seem too hot when compared with TRACE loops. Lowering the wave amplitudes does not solve this discrepancy, introducing magnetic twist will make the comparison even less desirable. We conclude that the nanoflare heating scenario better explains ultraviolet loops, while turbulence-based steady heating mechanisms may be at work in heating a fraction of soft X-ray loops.

1. Modeling solar coronal loops

How the solar corona is heated to multi-million degrees of Kelvin remains a topic of intensive study (Klimchuk 2006; Parnell & De Moortel 2012). Due to their higher demand of energy flux consumption (e.g., Withbroe & Noyes 1977), loop structures – the magnetically closed part of the corona – receive more attention than coronal holes – their magnetically open counterpart. Conventionally loop heating mechanisms are grouped into two categories: DC ones that involve the dissipation of the energy of the magnetic field stressed by supergranular motions most likely via magnetic reconnections at small scale current sheets, and AC ones that involve the deposition of energy that ultimately derives also from supergranular motions but is transported as waves.

Actually the fast solar wind that emanates from coronal holes also requires a basal heating. Their origin, originally attributed to the vaguely defined “coronal base” where the temperature has reached a million degree, has been observationally tracked down to the atmospheric layers above chromospheric network (Hassler et al. 1999; Tu et al. 2005). Not only supplying the required mass, the chromospheric activities may also provide the required energy for heating and transporting the materials from the upper

chromosphere to the corona (McIntosh et al. 2011). Stimulated by these measurements, modern fluid models of the solar wind tend to place the inflow boundary at the transition region or the upper chromosphere or even at photospheric levels (e.g., Cranmer 2012). To provide the needed heating for the nascent fast solar wind, modern models tend to use either observationally based empirical heating functions, or the heating rates due to the dissipation of various waves via, say, turbulent means.

It seems natural but in fact rather rare to see coronal loop models heated by mechanisms originally devised for heating nascent solar winds. The available ones are mainly based on the resonant interactions between protons and ion-cyclotron waves, which were designed in the solar wind context to naturally account for the temperature measurements above coronal holes, especially the inferred significant ion temperature anisotropy (e.g., Hollweg & Isenberg 2002). The needed ion-cyclotron waves may be generated either by a turbulent parallel cascade from low-frequency Alfvén waves emitted by the Sun (Li & Habbal 2003; O’Neill & Li 2005), or directly by small-scale magnetic reconnection events at chromospheric network (Bourouaine et al. 2008). While by construction the waves heat protons only, electrons may readily receive part of the heating via frequent collisions with protons given the high loop densities. These ion-cyclotron resonance based mechanisms were shown to be able to produce a million-degree loop with realistic densities. A salient feature of these models is that, when only unidirectional waves are introduced, the heating is generally not symmetric with respect to the looptop, resulting in substantial loop flows. These flows are essential in enhancing the loop densities relative to hydrostatic expectations. In parallel-cascade based models, it was also shown that the ponderomotive force density associated with the Alfvén waves plays an important role in the loop dynamics, especially close to the loop ends (Li & Habbal 2003). When magnetic twist is introduced, the electron temperature may be significantly enhanced due to the projection effect (Li & Li 2006).

In contrast to the extensive attempts in the loop community to directly contrast model computations with observations (e.g., Winebarger et al. 2003), the loop models using solar wind heating mechanisms have not been tested against observations. Of particular interest would be the loop density and temperature, which are the most frequently measured parameters. In this presentation we will present a preliminary study along this line of thinking. Specifically, the data that will be compared with are obtained by the ultraviolet instruments onboard TRACE and the X-ray instrument SXT onboard YOHKOH as compiled in Winebarger et al. (2003). We note that the filter ratio technique in deducing the temperatures may be subject to considerable uncertainty, however, let us only mention the limitations of the loop models here. The models are based on the parallel-cascade scenario where the Alfvén waves are injected at one loop end, and via a parallel cascade the wave energy is transferred to the ion-cyclotron range and therefore readily picked up by protons via proton cyclotron resonance (Hollweg & Isenberg 2002; Li & Habbal 2003). By using unidirectional waves described by a WKB-like equation supplemented with dissipation, we assume that the backward propagating waves, which are essential in generating any MHD cascade, do not contribute significantly to the energy flux density. In this sense the wave frequencies are higher than the Alfvén speed divided by its characteristic spatial scale. For the computed values it was found that this frequency would be of the order of one hundred Hertz, which seems high but consistent with the estimated frequencies of the Alfvén waves launched by chromospheric magnetic reconnections (Sturrock 1999). In future a more self-consistent treatment of bi-directional waves and their dissipation due

to mutual coupling should be pursued, say, in the manner proposed by Sokolov et al. (2013).

2. Model description

We approximate coronal loops as a semi-circular torus with length L and cross-sectional area a . The loop magnetic field B as a function of arclength l , measured from one loop footpoint along the axis, is related to a via $B \propto 1/a$. The loop material consists of electrons (e) and protons (p), and each species s ($s = e, p$) is characterized by its number density n_s , mass density $\rho_s = n_s m_s$, temperature T_s , velocity \mathbf{v}_s , and partial pressure $p_s = n_s k_B T_s$ with k_B being the Boltzmann constant. Quasi-neutrality ($n_e = n_p = n$) and quasi-zero-current ($\mathbf{v}_e = \mathbf{v}_p = \mathbf{v}$) are assumed. Only monolithic loops in steady state are considered, i.e., $\partial/\partial t = 0$, and the variation in the direction perpendicular to the loop axis is neglected. With electron inertia further neglected, the standard two-fluid MHD equations are then projected along the loop axis, rendering l the only independent variable. The governing equations read (for more details, please see Li & Habbal 2003)

$$(nva)' = 0, \quad (1)$$

$$v v' = -\frac{(p_e + p_p)'}{\rho} - g_{\parallel} + \frac{F}{\rho}, \quad (2)$$

$$v(T_e)' + \frac{(\gamma - 1)T_e(av)'}{a} = \frac{\gamma - 1}{nk_B a} (a\kappa_{e0}T_e^{5/2}T_e')' - 2\nu_{pe}(T_e - T_p) - \frac{\gamma - 1}{nk_B} L_{\text{rad}}, \quad (3)$$

$$v(T_p)' + \frac{(\gamma - 1)T_p(av)'}{a} = \frac{\gamma - 1}{nk_B a} (a\kappa_{p0}T_p^{5/2}T_p')' + 2\nu_{pe}(T_e - T_p) + \frac{\gamma - 1}{nk_B} Q_{\text{wav}}, \quad (4)$$

in which the prime ' denotes the differentiation with respect to l , and $\gamma = 5/3$ is the adiabatic index. Furthermore, $\rho = \rho_p$ is the total mass density, and g_{\parallel} denotes the gravitational acceleration corrected for loop curvature. The Coulomb collision rate ν_{pe} is evaluated by using a Coulomb logarithm of 23. The electron energy loss is denoted by L_{rad} , and we adopt the standard parametrization by Rosner et al. (1978) for an optically thin medium. Besides, $\kappa_{e0} = 7.8 \times 10^{-7}$ and $\kappa_{p0} = 3.2 \times 10^{-8}$ represent the Spitzer values for the species thermal conductivities (cgs units will be used throughout). By construction the energy deposition Q_{wav} due to waves goes entirely to heating protons, and is related to the wave evolution via

$$\frac{(aF_w)'}{a} + vF = -Q_{\text{wav}}, \quad (5)$$

where $F = -p_w'$ and F_w are the wave force and energy flux densities, respectively. Consistent with previous solar wind models, here Q_{wav} is assumed to follow a Kolmogorov rate, $Q_{\text{wav}} = \rho \xi^3 / L_{\text{corr}}$, where ξ denotes the wave amplitude, and L_{corr} denotes the correlation length associated with turbulent heating. As conventionally assumed, L_{corr} is proportional to $1/\sqrt{B}$ (Hollweg & Isenberg 2002).

Now we need to specify the axial distribution of the loop magnetic field strength $B(l)$, which is assumed to be symmetric about the looptop ($l = L/2$). We distinguish between two profiles, in one of which $B \equiv 60$ G is uniform and in the other it decreases from 240 G at loop ends to 60 G at looptop with the specific profile parametrized following the measurements of the loop cross-sectional area, deduced from the width

of supergranular network at a range of Ultraviolet lines formed at different temperatures (Aiouaz & Rast 2006).

The following boundary conditions are used. At both ends ($l = 0$ and L), the number density n and speed v are allowed to change freely, mimicking the filling and draining of loop materials due to coupling with the underlying denser layer. However, both electron and proton temperatures are fixed at 2×10^4 K, corresponding to the top of the chromosphere. The wave amplitude ξ_0 at the driving end ($l = 0$) where the waves enter the loop is 10 km/s, in line with the SUMER measurements with linewidths (Chae et al. 1998), but is allowed to vary freely at the outflowing end ($l = L$). As such, a solution is uniquely determined once one specifies the loop length L and the correlation length l_0 at the driving end, enabling us to perform a parametric study on the range the loops parameters may span at a range of loop lengths.

A description of the axial profiles of loop parameters is necessary (for details, see O'Neill & Li 2005). At a given L , for all the chosen l_0 the electron density n decreases from some chromospheric value at the driving end, attains a minimum, and then increases again towards a chromospheric value at the other end. The associated proton speed v and electron temperature T_e exhibit an opposite fashion. Their specific profiles critically depend on the choice of l_0 , with the tendency being that when l_0 increases, the wave heating becomes more uniform and the loop becomes less dynamic, i.e., the maximum speed decreases. If l_0 is larger than some critical value, the loop becomes static and there is practically no flow at all. If on the contrary l_0 is smaller than a critical value, the loop is so dynamic that a slow shock develops at one end. The shocked solutions may be important on theoretical grounds, but their observational detection in coronal loops has not been reported. We therefore are left with a range of l_0 , only in which the solutions are observationally accessible. Varying l_0 in this range, we find for any given L the ranges for the minimal electron density n_{Min} and maximum electron temperature T_{Max} , which are then compared with observations.

3. Comparison of model results with SXT and TRACE observations

Figure 1 presents the results from this parametric survey, which displays the computed ranges for n_{Min} and T_{Max} as a function of looplength L . The red crosses are the measured values for the TRACE (left column) and YOHKOH/SXT (right) loops, read from Tables 1 and 2 compiled by Winebarger et al. (2003). The black dashed curves are for the computations where the loop magnetic field is uniform, whereas the blue curves are for the case where loops experience some expansion. Specific computations are represented by the asterisks. It is clear from the figure that while varying the loop cross-section may drastically change the axial profiles of the loop parameters (not shown), the ranges the electron densities and temperatures may span are not substantially different: the ranges are slightly broader in the expanding case. From the left column, it is clear that while the electron densities measured by TRACE are reproduced remarkably well, the computed loops are too hot compared with measurements. In fact, among the 22 loops with lengths ranging from 30 to 300 Mm, literally all the measured values lie in the computed n_{Min} ranges, whereas only 3 lie in the computed T_{Max} ranges. An intuitive idea would that if we decrease the wave amplitude, this comparison would be more desirable, but this turns out not to be the case: lowering ξ_0 to 7 km/s, we found the computed loop temperatures are still too high. If introducing magnetic twist, which is often observed to be present in coronal loops, we would find that the loops are

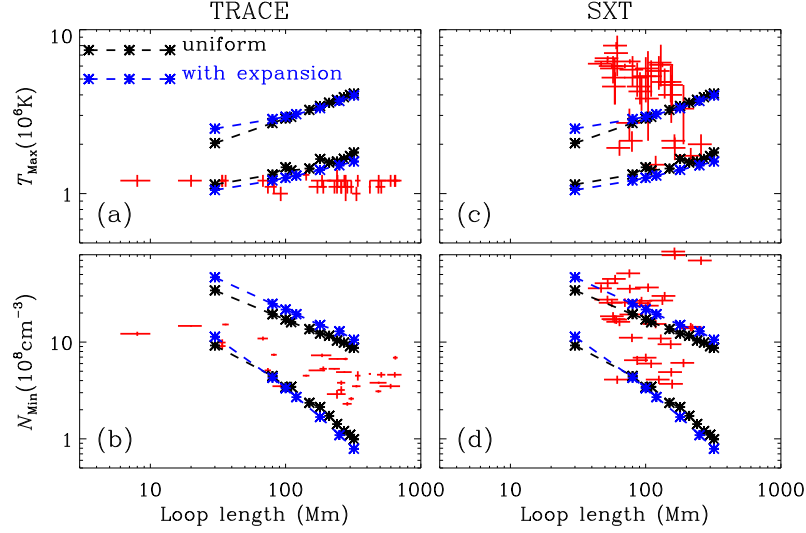


Figure 1. Comparison with measurements of loop parameters from models based on parallel cascade of Alfvén waves. Panels (a) and (b) display the computed range of the electron temperature maximum T_{Max} as a function of looplength. Likewise, panels (c) and (d) give the corresponding distribution of the ranges of the minimum electron density N_{Min} . The black dashed lines represent model computations where the loop cross-sectional area does not vary with distance, while the blue ones are for models where the loop experience some lateral expansion. Besides, the red crosses in the left (right) column display the parameters of the loops measured with TRACE (YOHKOH/SXT).

even hotter (Li & Li 2006). So we conclude here that at this level of sophistication, the parallel-cascade based mechanisms cannot explain the EUV loops, whose flat distribution of temperatures just above 1 MK may be better explained by the impulsive heating scenarios, e.g., the nanoflare approach.

The computed loop parameters compare more favorably with SXT measurements. While not perfectly reproduced, among the 47 loops measured, 10 loops lie in the computed T_{Max} ranges, with an additional 3 being possible when the measurement uncertainty is considered. As for the loop densities, 20 of the measured values lie in the computed ranges. From this we conclude that the steady heating model based on this parallel cascade scenario may account for a substantial fraction of the soft X-ray loops. Interestingly, there is observational evidence that the X-ray emitting Active Region cores may last hours, thereby partly lending support to some steady heating.

4. Summary

The problem of coronal heating largely concerns the question of how to heat the magnetically closed part of the Sun – coronal loops – to multi-million degrees of Kelvin. However, there is ample evidence that the solar wind, at least the fast streams, originates from the atmospheric layers as low as the top of the chromosphere, and therefore has to undergo some basal heating to bring their temperature to a million degree as well. In this sense it is worth examining whether the mechanisms designed for heating the

nascent fast solar wind can be also applied to coronal loop heating. This was undertaken by Li & Habbal (2003); O'Neill & Li (2005); Li & Li (2006); Bourouaine et al. (2008). Somehow these attempts still lack a rigorous observational test: there is neither an attempt to reproduce a particular observed loop, nor a study to examine whether the proposed mechanisms can reproduce the observed loop ensembles with different instruments. We present a preliminary attempt that falls in the second category, examining the applicability of parallel-cascade based mechanisms where ion-cyclotron resonance plays the central role. However, we found that with the observationally constrained wave amplitudes, this mechanism cannot reproduce the TRACE loops, for the computed loop temperatures are always higher than observed. Nonetheless, the computed loop densities and temperatures can reproduce a substantial fraction of the SXT loops. Given that the solar wind studies have accumulated a considerable set of mechanisms, a serious need exists to test their applicability to loop heating in a systematic manner against observations, such as was conducted in the present study.

Before closing, we note that the conclusions drawn here apply only to the parallel-cascade scenario. It remains to be seen whether perpendicular-cascade-based mechanisms, now intensively pursued in the solar wind community (e.g., Chandran et al. 2011; Li & Habbal 2013), can reproduce the ultraviolet observations of coronal loops. Such a study, however, is left for a future publication.

Acknowledgments. This research is supported by the 973 program 2012CB825601, the National Natural Science Foundation of China (40904047, 41174154, 41274176, and 41274178), and by the Ministry of Education of China (20110131110058 and NCET-11-0305).

References

- Aiouaz, T., & Rast, M. P. 2006, *ApJ*, 647, L183
 Bourouaine, S., Vocks, C., & Marsch, E. 2008, *ApJ*, 676, 1346
 Chae, J., Schühle, U., & Lemaire, P. 1998, *ApJ*, 505, 957
 Chandran, B. D. G., Dennis, T. J., Quataert, E., & Bale, S. D. 2011, *ApJ*, 743, 197. 1110.3029
 Cranmer, S. R. 2012, *Space Sci. Rev.*, 172, 145. 1007.0954
 Hassler, D. M., Dammasch, I. E., Lemaire, P., Brekke, P., Curdt, W., Mason, H. E., Vial, J.-C., & Wilhelm, K. 1999, *Science*, 283, 810
 Hollweg, J. V., & Isenberg, P. A. 2002, *Journal of Geophysical Research (Space Physics)*, 107, 1147
 Klimchuk, J. A. 2006, *Solar Phys.*, 234, 41. astro-ph/0511841
 Li, B., & Habbal, S. R. 2013, in *Numerical Modeling of Space Plasma Flows (ASTRONUM2012)*, edited by N. V. Pogorelov, E. Audit, & G. P. Zank, vol. 474 of *Astronomical Society of the Pacific Conference Series*, 153. 1211.7136
 Li, B., & Li, X. 2006, *Royal Society of London Philosophical Transactions Series A*, 364, 533
 Li, X., & Habbal, S. R. 2003, *ApJ*, 598, L125
 McIntosh, S. W., Leamon, R. J., & De Pontieu, B. 2011, *ApJ*, 727, 7. 1011.3066
 O'Neill, I., & Li, X. 2005, *A&A*, 435, 1159
 Parnell, C. E., & De Moortel, I. 2012, *Royal Society of London Philosophical Transactions Series A*, 370, 3217. 1206.6097
 Rosner, R., Tucker, W. H., & Vaiana, G. S. 1978, *ApJ*, 220, 643
 Sokolov, I. V., van der Holst, B., Oran, R., Downs, C., Roussev, I. I., Jin, M., Manchester, W. B., IV, Evans, R. M., & Gombosi, T. I. 2013, *ApJ*, 764, 23. 1208.3141
 Sturrock, P. A. 1999, *ApJ*, 521, 451
 Tu, C.-Y., Zhou, C., Marsch, E., Xia, L.-D., Zhao, L., Wang, J.-X., & Wilhelm, K. 2005, *Science*, 308, 519

- Winebarger, A. R., Warren, H. P., & Mariska, J. T. 2003, ApJ, 587, 439
Withbroe, G. L., & Noyes, R. W. 1977, ARA&A, 15, 363